Solar Tides as Revealed by Measurements of Mesosphere Temperature by the MLS Experiment on UARS

Jeffrey M. Forbes (forbes@colorado.edu)

Department of Aerospace Engineering Sciences, University of Colorado, Boulder, CO

Dong Wu (dwu@mls.jpl.nasa.gov)

Jet Propulsion Laboratory, Pasadena, CA

Abstract

Temperatures between 25 and 86 km measured by the Microwave Limb Sounder (MLS) experiment on the Upper Atmosphere Research Satellite (UARS) are analyzed to delineate diurnal, semidiurnal and terdiurnal tidal structures and stationary planetary waves. These Fourier components are determined from temperatures averaged in bins covering 5° latitude, 30° longitude and 1 hour in local time. This study confirms the presence of diurnal non-migrating tides with zonal wavenumbers s = 0, 2, -3 [s > 0 (s < 0) implying westward (eastward) propagation] and semidiurnal tides with s = 1 and 3, and some components of lesser importance, that were previously determined from UARS wind measurements near 95 km. The seasonal-latitudinal and height structures of these components are now revealed, and utilized to aid in interpreting their behaviors and ascertaining their origins. New discoveries include the terdiurnal s = 2 and s = 4 components, and trapped non-migrating diurnal tides with s = 0 and s = 2. The former

are likely to arise from nonlinear interaction between the migrating (s = 3) terdiurnal tide and the stationary planetary wave with s = 1. The latter may reflect the presence of a longitude-dependent local heat source, or nonlinear interaction between migrating diurnal tidal fields driven by such a source, with local fields associated with a stationary planetary wave with s = 1. The present results provide a rich mixture of observational results to challenge both mechanistic and general circulation models of the middle atmosphere. In addition, internal consistency is established between the MLS tidal temperatures at 86 km and previously derived tidal winds at 95 km within the context of tidal theory. Although not definitive, this result is consistent with no bias in the UARS/HRDI winds at 95 km, suggesting that source of the well-known inconsistency between winds measured from the ground and space to primarily reside in the radar wind measurements.

1. Introduction

The global temperature, density and wind fields induced by the daily cyclic absorption of solar energy in an atmosphere are referred to as solar thermal tides. Assuming continuity in space and time around a latitude circle, solar thermal tidal fields are represented in the form

$$A_{n,s}\cos\left(n\Omega t + s\lambda - \phi_{n,s}\right) \qquad (1)$$

where t = time (days), Ω = rotation rate of the earth = 2π day^{-1}, λ = longitude, n (= 1, 2, ...) denotes a subharmonic of a solar day, s (= .... -3, -2, ...0, 1, 2, ...) is the zonal wavenumber, and the amplitude $A_{n,s}$ and phase $\phi_{n,s}$ are functions of height and latitude. In this context, n = 1,2,3 represent oscillations with periods corresponding to 24 hours, 12 hours, 8 hours, and hence are referred to as diurnal, semidiurnal and terdiurnal tides,

respectively. Eastward (westward) propagation corresponds to $s < 0$ ($s > 0$). The phase is defined as the time of maximum at zero longitude; in other words, the local time at Greenwich. (The alternative definition of longitude of maximum at t = 0 is not used for tides, since the phase is undefined for $s = 0$). At any height and latitude the total tidal response is obtained as a sum over n and s.

Rewriting (1) in terms of local time $t_{LT} = t + \lambda/2\pi$, we have

$$A_{n,s} \cos\left[n\Omega t_{LT} + (s-n)\lambda - \phi_{n,s} \right] \qquad (2)$$

Solar radiation absorption by a zonally symmetric atmosphere or surface yields daily (local time) variations that are independent of longitude, i.e., $s = n$. From (1) such components correspond to a zonal phase speed $C_{ph} = d\lambda/dt = - n\Omega/s = -\Omega$, in other words westward-propagating at the same speed as the apparent motion or ``migration'' of the Sun to a ground-based observer. These sun-synchronous tidal components are referred to as ``migrating'' tides.

Now consider the cyclic heating due to absorption of solar energy by a zonally asymmetric (longitude-dependent) planetary atmosphere or surface. In response to this heating, the local time structure of the atmosphere (at a given height and latitude) is dependent on longitude. A common approach is to examine zonal wavenumber spectra of the lowest-order local time harmonics (diurnal, semidiurnal, terdiurnal) that combine to give rise to the salient features of this longitude dependence. In this case, Fourier representation must involve a range of zonal wavenumbers of both sign, corresponding to waves propagating to the east ($s < 0$) or west ($s > 0$) (Chapman and Lindzen 1970). This approach offers the opportunity to relate results to tidal theory and numerical models, and often to gain physical insight. While some examples of longitudinally-varying local time

structures are illustrated in this paper, emphasis herein is focused on analysis and interpretation of the Fourier components of the temperature field.

Throughout the remainder of this paper we utilize the notation and DWs or DEs to denote a westward or eastward-propagating diurnal tide, respectively, with zonal wavenumber s. For semidiurnal and terdiurnal oscillations 'S' and 'T' replaces 'D'. The standing oscillations are denoted D0, S0, T0, and stationary planetary waves with zonal wavenumber m are expressed as SPWm.

While non-migrating tides were known to exist in surface pressure observations (Chapman and Lindzen 1970), their unambiguous identification in the mesosphere and lower thermosphere was not possible until the advent of global satellite measurements at altitudes where the tidal signal is sufficiently large in comparison to other sources of variability (i.e., Lieberman 1991; Hagan et al. 1997b; Talaat and Lieberman 1999; Manson et al. 2002; Oberheide and Gusev, 2002; Forbes et al. 2003). These studies were hampered by local time sampling limitations, thus severely affecting the altitude or latitude regime of the tidal determinations, the tidal period capable of being ascertained, or introducing aliasing uncertainties into the analyses. Nevertheless, the available observational analyses spawned a number of modeling investigations seeking to explain the origins and characteristics of nonmigrating tides in the mesosphere and lower thermosphere (i.e., Ekanayake et al. 1997; Miyahara et al. 1999; Forbes et al. 2001; Hagan and Roble, 2001; Grieger et al., 2002; Hagan and Forbes 2002, 2003). It is now generally accepted that non-migrating tides in the upper atmosphere arise from at least two mechanisms: zonally asymmetric thermal forcing, and nonlinear interactions among tides and SPWs. For instance, it is well known that latent heating associated with deep

tropical convection possesses strong variations with U.T., longitude, latitude and season. Studies by Hagan et al. (1997a), Forbes et al. (1997, 2001), Hagan and Forbes (2002, 2003) and Oberheide et al. (2002) demonstrate that this source of excitation leads to diurnal and semidiurnal tides over a spectrum of zonal wavenumbers that propagate into the mesosphere and thermosphere and achieve significant amplitudes in this height regime.

Much evidence now exists that supports nonlinear wave-wave interactions as an important source of nonmigrating tides. The mechanism works as follows (Teitelbaum and Vial, 1991). Given two oscillations with respective frequency-zonal wavenumber pairs (σ_1, σ_1) and (s_1, s_2), and under the assumption of a so-called quadratic interaction between these two 'primary waves', and neglecting self-interactions, "sum and difference" secondary waves are generated with the frequency, zonal wavenumber pairs ($\sigma_1 + \sigma_2$, $s_1 + s_2$) and ($\sigma_1 - \sigma_2$, $s_1 - s_2$). Teitelbaum and Vial (1991) invoked this mechanism as a secondary means (beyond direct solar heating) of exciting the migrating terdiurnal tide (n = 3, s = 3), via interaction between the migrating diurnal (n = 1, s = 1) and semidiurnal (n = 2, s = 2) tides. These mechanisms for exciting the terdiurnal tide have recently been considered by Smith (2000) and Smith and Ortland (2001). Forbes et al. (1995) suggested nonlinear interaction between SW2 and SPW1 to explain existence of a large SW1 tide over South Pole. Recent modeling work in fact indicates that nonlinear interactions between SPW1 and migrating tides lead to significant nonmigrating diurnal and semidiurnal tidal signatures above about 80 km altitude (Hagan and Roble, 2001; Yamashita et al., 2002; Angelats i Coll and Forbes, 2002; Lieberman et al., 2004; Grieger et al., 2004). There are of course many other combinations of tide-tide

and tide-planetary wave interactions that may be effective in producing observable nonmigrating tidal signatures in the upper atmosphere. It is also arguable that the interaction of a zonally-asymmetric distribution of gravity waves interacting with migrating tides could also generate nonmigrating tidal components.

The purpose of the present work is to explore the temperature measurements made by the Microwave Limb Sounder (MLS) instrument on UARS to establish the degree of longitude variability in the local time temperature structure, and to identify the primary non-migrating tidal components responsible for the longitude variability. Similar analyses have been performed on UARS wind measurements (Forbes et al., 2003); however, that study was restricted to 95 km and ±42° latitude where both day and night data were available to perform unambiguous separation between tidal components that could potentially alias into one another. Advantages of the MLS temperature measurements for this type of study include wider latitude coverage due to the nature of the instrumental sampling, and 24-hour local time coverage over the ~25-86 km altitude range, thus allowing examination of vertical structures. The upper altitude limit of 86 km means, however, that the tidal amplitudes that we are seeking to identify have not yet achieved their altitude of maximum amplitude (ca 110-150 km) and may be relatively small, thus admitting potential contamination from other temperature variations.

2. The Experimental Data and Method of Analysis

The data analyzed here consist of temperatures between 20 and 86 km derived from 63 GHz O_2 emissions measured by the Microwave Limb Sounder (MLS) on the Upper Atmosphere Research Satellite (UARS). Descriptions of the experimental technique, instrument sampling, the retrieval algorithm and information on precision and validation

are provided in Wu et al. (2003). The estimated precision of MLS temperatures varies from 1.5-4.0 K between 20-60 km and 6.0-8.0 K between 60-85 km and increases sharply above 90 km. Comparisons with other data sets suggest biases at some altitudes, but these are not expected to significantly affect the temperature *variations* described here.

Because the instrument views 90° to the satellite velocity vector in a 585 km and 57° inclination orbit, MLS latitude coverage on a given day extends from 34° in one hemisphere to 80° in the other. The satellite executes a 180° yaw maneuver 10 times a year, yielding alternative views of high latitudes every 36 days. The MLS experiment collected temperatures from September 1991 – June 1997, with superior and near-continuous coverage during 1 November – 27 October 1994. The latter period is selected for the present analysis, due to its uniformity in longitude and U.T. sampling.

The temperature data were analyzed as follows to extract the tidal components, which represent 3-year averages over the 1 November 1991 – 27 October 1994 period. Within each fitting interval (see below) temperatures were averaged in bins spanning 24° longitude, 5° latitude, and 1 hour in U.T. at increments of 2 km altitude from 20 to 86 km. A standard deviation was computed for each hourly data point, primarily providing a measure of geophysical variability. At each altitude, latitude and longitude, Fourier least-squares fits were performed with respect to U.T. to determine amplitudes and phases of diurnal, semidiurnal and terdiurnal tidal components. Each frequency component was then subjected to Fast Fourier Transform (FFT) to perform the zonal wavenumber decomposition for s = -6 to s = +6. Average temperatures in the longitude and U.T. bins were also subjected to a two-dimensional FFT, determining the frequency and zonal wavenumber decompositions simultaneously, with little change in the results. At each

stage in the analysis, 1-sigma uncertainty estimates in the Fourier-component amplitudes and phases were computed, and propagated forward from the initial standard deviations in the hourly average data through subsequent stages of the analysis.

The above sampling and binning procedure must be set into the context of the constraints of instrument sampling imposed by the yaw cycle maneuvers. Figure 1 illustrates the spatial-temporal coverage for the MLS temperature data covering the complete 1 November 1991 – 27 October 1994 data interval; as such, it is slightly different than the yaw cycle coverage for any given year. Our time intervals for binning of data in local time are centered on the 15th of each month, and span 36 days at latitudes equatorward of ±34°, and 72 days at higher latitudes. This ensures 24 hours of local time coverage at all latitudes between ±80°. At latitudes poleward of ±34° the high-latitude sampling during many months (i.e., January, April, June, November in the S. Hemisphere, and May, July, October, December in the N. Hemisphere) consists of ~36 continuous days such that they overlap most of the same month-days as the sampling equatorward of ±34°. On the other hand, there are some months (i.e., February, March in the S. Hemisphere and August, September in the N. Hemisphere) where the 36 days of high-latitude data coverage are "continuous", but are centered near the beginning or end of an adjacent month (i.e., slipped ~18 days from mid-month). There are also some months (i.e., May and December in the S. Hemisphere and November, January in the N. Hemisphere), where the 15th of the month falls in the gap between yaw cycles, and about half the local times binned together originate in the previous and following yaw cycles. It is these latter months (in one hemisphere or the other) that may be most subject to aliasing of the type discussed in the appendix. However, the reader is reminded that the

results described here are climatological in the sense that they represent multi-year averages. We have chosen to analyze the data in this fashion, rather than on a yaw cycle by yaw cycle basis, in order to obtain a data product that spans both hemispheres up to ±80° without alternating data gaps between the yaw cycles. The multi-year averaging utilized here should ameliorate the shortcomings associated with this chosen methodology.

As is evident from Equation (2), from sun-synchronous orbit (t_{LT} = constant), all waves with the same value of (s-n) are indistinguishable from each other, in other words, they alias into each other. In the present context, this includes stationary planetary waves (n = 0, s = 1), diurnal tides (n = 1) with s = 0 and s = 2; semidiurnal tides (n = 2) with s = 1 and s = 3; and terdiurnal tides (n = 3) with s = 2 and s = 4. As satellite sampling precesses through local time, these aliasing effects are expected to decrease and ultimately disappear until all waves are fully sampled; that is all local times are sampled at all longitudes. In the present method, where we utilize 3-year climatological averages filling all longitude and U.T. bins several times over at a given height and latitude, we expect our space-time decomposition to be alias-free. Multi-year and monthly averaging also has the tendency to underestimate amplitudes when the dynamical fields exhibit year-to-year variability or non-stationarity during the fitting interval. It is difficult to assess the impact of these effects, but any future attempts at comparing model outputs with our results should address this problem through appropriate averaging of the model fields.

In at least two cases, non-stationarity of the dynamical fields can also lead to aliasing effects. For instance, an SPW1 that evolves during the fitting interval can alias into all

of the nonmigrating tidal components mentioned in the previous paragraph. This is demonstrated in the appendix, where we provide estimates of the potential effects. In addition, as shown by Forbes et al. (1997), a time-varying zonal mean field can alias into the migrating (sun-synchronous) tidal components, since from the satellite perspective it is not possible to distinguish between a true local time variation, and a zonal mean variation that projects onto the local time precessing frame of the satellite. It is possible to greatly reduce this effect by taking (for the UARS satellite) a 36-day running mean through the data, subtracting this running mean from the original data, and then analyzing the residuals to extract the tidal components (Forbes et al., 1997). However, it is only possible to apply this method when the data are continuous in time (i.e., not subject to yaw maneuvers). For the present data, we applied this method equatorward of ±34° latitude, and verified that nearly equivalent results were obtained for the binning method reported here. We suspect that the binning method (without removal of the running mean) may be more problematic when applied to a satellite that takes much longer than 36 days to precess in local time, i.e., for instance the 60-day precession period of the TIMED satellite.

3. Local Time Structures

Given that the present study focuses on solar thermal tides, it is natural to first examine the temperature structures revealed by the MLS experiment ordered in local time. Figure 2 provides plots of hourly temperatures at 86 km versus local time, at 0° and –60° latitude and at six longitudes between 12°E and 300°E for the month of March. These data are typical of other months as well. Each point corresponds to a one-hour average as described in Section 1, and the vertical lines represent 1-sigma standard

deviations corresponding to the mean values in each local time bin. This figure also offers an opportunity to provide a measure of the geophysical variability in the data, as manifested in the displayed standard deviations. The solid lines in Figure 1 represent least-squares fits corresponding to superposition of diurnal, semidiurnal and terdiurnal Fourier harmonics. It is readily apparent that the local time structures as well as mean values vary significantly with longitude; the former implies the existence of nonmigrating tides, the latter with stationary planetary waves. The changes in local time structure with longitude imply the presence of diurnal, semidiurnal and perhaps terdiurnal nonmigrating tides, as discussed in connection with Equation 2. The following sections primarily focus on the depiction of these tidal components and their interpretation.

4. Spectral Overview

As noted previously, at a given longitude the local time structure is reasonably approximated by a superposition of diurnal, semidiurnal and terdiurnal harmonics (i.e., n = 1, 2, 3 in Equation 2). The variation with longitude of the local time structure is embodied in a spectrum of zonal wavenumbers (i.e., s-values in Equation 2) for each nth harmonic. In theory an infinite sum is required to capture the longitude variation of each harmonic, but in practice relatively few harmonics are found to dominate. This point is illustrated in Figure 3, wherein power spectra (i.e., square of temperature amplitude) are illustrated for stationary planetary waves, and the diurnal, semidiurnal and terdiurnal nonmigrating tidal components, for July and January at 86 km. Migrating tides are omitted from this figure in order to highlight the smaller-amplitude nonmigrating components.

Figure 3 also provides insight into potential sources for the observed nonmigrating

tides. For instance, it is now generally accepted (i.e., Conrath, 1976; Zurek, 1976; Tokioka and Yagai, 1987; Yagai, 1989; Hendon and Woodberry, 1993; Williams and Avery, 1996; Forbes et al., 2001) that to first order zonal asymmetries in surface or atmospheric properties characterized by zonal wavenumber m modulate absorption of the nth harmonic of diurnally-varying solar radiation to excite the "sum and difference" thermal tides with frequency $n\Omega$ and zonal wavenumbers $n \pm m$. Existence of DW2 and D0 in Figure 3 is thus consistent with nonlinear interaction between DW1 and SPW1 (Hagan and Roble 2001) although these components can also be excited by latent heating in the troposphere, wherein a similar interaction between the DW1 component of solar radiation and the s = 1 component of topography/land-sea contrast exists (Hagan and Forbes, 2002). Similar interactions between SW2 (TW3) with SPW1 or s = 1 topography, lead to SW1 and SW3 (TW2 and TW4) tidal components that also figure prominently in the power spectrum of Figure 3. The SDE2 and SW6 pair are consistent with modulation of SW2 radiation absorption by the m = 4 component of topography/land-sea contrast, which is dominant at low latitudes (Yagai, 1989). Most likely, the DE2 and DE3 components evident in Figure 4 are directly forced in the troposphere by latent heating (Forbes et al., 2001). These tidal components have significantly longer vertical wavelengths than their westward-propagating counterparts, are thus less susceptible to dissipation, and hence more likely to penetrate to the upper mesosphere/lower thermosphere (Ekanayake, et al., 1997).

During July, the SPW1 maximum in Figure 3 is in the S. Hemisphere, as are SW1, SW3, D0 and DW2. However, as the SPW1 maximum shifts to N. Hemisphere winter, maxima of SW1 and SW3 shift to the same hemisphere, but the diurnal non-migrating

tides provide little evidence for a shift into the N, Hemisphere, and instead show an intensification at high summer latitudes. This perhaps suggests some difference in the atmospheric region or mechanism by which the diurnal and semidiurnal non-migrating tides are generated.

Figure 4 provides a height versus month perspective on the amplitude structures of SPW1, D0, DW1, and DW2 at –60° latitude. While SPW1 exhibits maximum values during late local winter, the amplitude of DW2 is virtually nil below 60 km, and only ~1.0 K below 50 km for D0. In the latter case it is reasonable to argue that some of the upper-level (> 50 km) response is due to zonally symmetric tides propagating upward from a nonlinear interaction region below, since according to classical tidal theory the D0 temperature response is nonzero at the poles for the fundamental propagating mode. However, for DW2 any response at –60° latitude must occur in connection with trapped components, and hence an in-situ source of excitation. Further, the lack of similarity between the SPW1 and DW2 amplitudes is consistent with the absence of the type of aliasing addressed in the Appendix. Note also that the diurnal non-migrating tides tend to show their largest amplitudes where signatures of *both* DW1 and SPW1 are relatively large, possibly reflecting the nonlinear generation of non-migrating tides in these regions. The counterpart of Figure 4 for the semidiurnal tide is provided in Figure 5, where height vs, month contours of temperature amplitude are depicted for SPW1, and for SW2, SW1 and SW3 at +60° latitude. Note that SW2 amplitudes are of order 2.0-4.0 K above 70km during all months except December and January, and between 25 and 70 km during most months except for May, June, July. SPW1 amplitudes are of order 4-10 K between 20 and 85 km, confined mainly to October through April. Based on these results, one would

expect the nonlinear generation of the "sum and difference" waves SW1 and SW3 to be confined to the height versus month regime of significant SPW1 amplitudes. Distributions of the SW1 and SW3 amplitudes are consistent with this. However, the alternate possibility of aliasing due to time evolution of the SPW1 amplitudes during the fitting intervals must be considered. According to our estimates in the Appendix, such effects should not exceed ~10% of SPW1 amplitudes, and tend to be confined to those time intervals where the SPW1 is evolving with time, i.e., February-April and September-November in Figure 5. Indeed, SW1 and SW3 amplitudes fall within 1-2 K (10-20% of SPW1) range and hence this possibility appears probable. Therefore, the following depictions of non-migrating tides will be confined to 86 km, where the amplitudes are generally largest and the aliasing effects due to SPW1 are minimized.

5. Hough components

It is sometimes illustrative to examine tidal structures in terms of Hough functions, the eigenfunctions of Laplace's tidal equation (Chapman and Lindzen 1970). In particular, for the diurnal tide, which consists of both propagating and trapped components, some insight into the possible existence of in-situ excitation may be revealed. In addition, the relative importance of various Hough functions for propagating components can also provide some insight into vertical structures by virtue of the connection between eigenfunctions, eigenvalues and vertical wavelengths (Chapman and Lindzen 1970).

Hough functions for the diurnal tides with s = 0, s = 1, s = 2 and s = 3 are provided in Figure 6. For each wavenumber, Hough functions for the first symmetric and antisymmetric propagating (index *m* positive in Figure 6) and trapped (index *m* negative) modes are displayed. In contrast to the other wavenumbers, note that (a) the fundamental

modes (m = +1 or –1) for s = 0 are antisymmetric instead of symmetric; (b) All s = 0 modes are nonzero at the poles; and (c) the trapped modes maximize at the poles. Note also the well-known characteristics of diurnal Hough functions: the propagating components maximize at low latitudes (<30°), whereas the trapped modes maximize at middle to high latitudes.

Figure 7 illustrates the amplitudes and phases of D0, DW1 and DW2 at 86 km (solid points with 1-σ standard deviations), along with fits (solid lines) obtained by reconstruction using the first four Hough modes for each zonal wavenumber. The D0 amplitudes are characterized by relatively high σ's, and no further interpretation will be attempted, although the coherence between independently-derived phases at different latitudes may be worthy of note. DW1 amplitudes maximize at about 9 K near the equator, reflecting dominance of the first symmetric propagating component of the diurnal oscillation. However, the broadness of this structure and to some degree the non-symmetric phase structure suggest the presence of higher-order modes. (Of course, much better agreement could be obtained by adding more Hough modes, as these functions form a complete orthogonal set.) The DW2 amplitudes are reasonably represented by the first four Hough modes. Examination of the Hough mode amplitudes reveals that the most important contributions to DW1 and DW2 are the first symmetric propagating modes, but that the trapped modes also make important contributions, as might be expected from the measured amplitudes at middle to high latitudes. This implies that part of the excitation lies at lower altitudes (see Introduction), but that there is an in-situ excitation mechanism for generating evanescent or trapped tidal components as well. One possibility might be broadening (i.e., 'mode coupling') due to dissipation in this

height regime (Lindzen and Hong, 1974; Lindzen et al., 1977; Forbes and Hagan, 1982). Another possibility is an in-situ heat source, possibly chemical heating (Mlynczak et al., 1993; Smith et al., 2003), which would likely only directly excite the migrating (Sun-synchronous) tide. The corresponding trapped components for D0 and DW2 could in principle result from in-situ nonlinear interaction between DW1 and SPW1. In principle, of course, D0 and DW2 could result from a longitude-dependent heat source as well, but there is no know evidence for expecting significant zonal asymmetries in the background atmospheric state at these altitudes.

Figure 8 provides a similar illustration for the s = 1, 2 and 3 semidiurnal tides for January at 86 km. For the semidiurnal tide, and the terdiurnal tidal component that will be discussed momentarily, we have only fit the first symmetric and first antisymmetric Hough modes to the data. Differences between the observations and fits displayed in Figure 8 therefore imply the existence of higher-order modes. The Sun-synchronous (s = 2) semidiurnal tide maximizes near 6 K at –10° latitude, and reflects significant differences between the 2-mode Hough reconstruction and the measurements at latitudes poleward of about ±30° latitude. This is not surprising, as the (2,4), (2,5) and even (2,6) Hough modes have often been cited as contributing to global semidiurnal tidal wind structures (Lindzen, 1976; Forbes et al., 1994; Forbes, 1982; Forbes and Vial, 1989, 1991). On the other hand, the SW1 and SW3 amplitude and phase structures are represented well by the first symmetric and anti-symmetric Hough modes. The amplitudes of these non-migrating tidal components maximize near 2.0 K, and depending on the latitude each attains values of order 30-50% of the migrating component.

The corresponding depiction for the terdiurnal tides is provided in Figure 9. Here the

amplitudes are smaller, of order 0.5 – 2.0 K, and subject to larger variability and relative errors. Some degree of coherence in phases between latitudes (and altitudes, not shown) lends some credibility to the existence of these structures as independent propagating oscillations. These oscillations are not important to the dynamics of the upper mesosphere. However, due to their long vertical wavelengths, they can be expected to achieve significant amplitudes in the 120-170 km region and above, and possibly contribute to the dynamo generation of electric fields and other aspects of the variability of the region. Since experimental data for the atmosphere above 100 km is particularly sparse, efforts like the present one, supplemented by tidal models or GCMs with lower boundaries in the mesosphere, can provide some insight into dynamical consequences at upper levels. In addition, the existence of non-migrating tidal oscillations can provide clues to nonlinear interactions that may be occurring at lower levels of the atmosphere.

6. Seasonal-Latitudinal Structures

A perspective on seasonal-latitudinal variability of the diurnal tidal oscillations is provided in Figure 10. Latitude versus month contours of diurnal temperature amplitudes at 86 km altitude for D0, DW1 and DW2 are depicted. Amplitudes for DW1 are of order 4-10 K, while that of D0 and DW2 are of order 1-4 K. DW1 exhibits maxima within the ±40° latitude regime that are primarily associated with propagating components, but significant amplitudes also exist at higher latitudes that reflect the presence of trapped components. Similar features are found in the amplitudes of D0 and DW2, but curiously, the high-latitude maxima are confined to the S. Hemisphere and show relatively little dependence on time of year. The diurnal tidal wind amplitudes for D0 at 95 km, as displayed in Forbes et al. (2003), also exhibit this same asymmetry between hemispheres,

but their results only extend to ±42° latitude. The origin of this latitudinal asymmetry remains unknown, but appears to be a real and persistent feature of the 85-95 km height region.

A similar depiction for the semidiurnal tidal component is provided in Figure 11. Amplitudes for the semidiurnal tide are generally of order 2-6 K for SW2 and 1-2 K for SW1 and SW3, i.e., roughly half of those of the diurnal tides depicted in Figure 10. SW1 and SW3 amplitudes tend to be confined to latitudes between ±40° latitude, whereas for SW2 large amplitudes occur at high latitudes during some seasons. This is consistent with the observation made in connection with Figure 8, that higher-order Hough modes (which tend to maximize at higher latitudes than the lower-order modes) are required to capture the latitude variations of SW2 than SW1 and SW3, which are adequately represented by a sum of the first symmetric and first antisymmetric Hough functions. For SW1, there are some ~1K amplitudes in the local winter seasons at middle to high latitudes in the N. and S. Hemispheres. At least in the S. Hemisphere, this amplitude distribution is different than what one would expect on the basis of wind observations near 94 km over South Pole (Forbes et al., 1995, 1999; Portnyagin et al., 1998), which indicate maximum SW1 meridional wind amplitudes during local summer. Modeling work is apparently needed to explain these differences.

DE3 is a prominent oscillation in the sample spectra of Figure 3. Modeling studies (Forbes et al., 2001; Hagan and Forbes, 2002) show that this oscillation is forced primarily by latent heat release due to deep tropical convection. DE3 was found to be the largest of all the non-migrating diurnal tidal components in the tidal analysis of UARS winds at 95 km by Talaat et al. (1999) and by Forbes et al. (2003). In this section we

present our results for DE3, and use a methodology involving Hough Mode Extensions (HMEs, Lindzen et al., 1977; Forbes and Hagan, 1982) to examine consistency with UARS DE3 *wind* determinations (Forbes et al., 2003) near *95 km*. As it turns out, this has some relevance to the controversy surrounding the differences between ground-based and space-based wind measurements near 95 km.

The temperature amplitude of DE3 as derived from the MLS data is plotted versus latitude and month in Figure 12. At these altitudes the maximum amplitude is about 2.5-3.0 K, significantly smaller than the maximum amplitude of 8 K for DW1, but during July DE3 is in fact stronger than DW1 at these altitudes. It is clear that during some months of the year the DE3 amplitude structure is very non-symmetric with respect to the equator, whereas during N. Hemisphere summer DE3 is predominantly symmetric with a Kelvin wave latitude structure. The degree of asymmetry during the various months is in fact consistent with the eastward and northward wind structures at 95 km displayed in Forbes et al. (2003). We will now examine the consistency between the temperature perturbations at 86 km and the wind perturbations at 95 km in a more quantitative way, which involves a set of basis functions called Hough Mode Extensions (HMEs). A brief description of HMEs will now be provided, and their use in providing new information on measurements in the MLT region will be explored. Due to the complications associated with trapped components in the DW1 and DW2 fields, and the large uncertainties in our D0 results, we will confine our attention concerning application of HMEs to the DE3.

The concept of Hough Mode Extensions was developed by Lindzen et al. (1977) and Forbes and Hagan (1982) in order to deal with the changes in shape of Hough Modes as

they encountered dissipation in an atmospheric regime above that of wave forcing. A Hough Mode Extension represents the solution to the linearized dynamical equations of the atmosphere taking into account dissipative effects above the forcing region. For a given *s* and σ, a HME can be thought of as a latitude vs. height table of amplitudes and phases for the velocity, temperature and density perturbation fields (*u, w, v, T, ρ*) of the oscillation. The u, w, v, T, ρ perturbation fields maintain internally self-consistent relative amplitude and phase relationships for any given HME. So, if the amplitude and phase of the perturbation wind field is known for a given HME at a single latitude and height, then all the fields, u, w, v, T, ρ are known for all latitudes and all heights. Svoboda et al. (2005) compute and utilize HMEs to fit UARS tidal winds at 95 km, and by reconstruction use the HMEs to arrive at an internally-consistent global climatology of tidal temperatures, winds and densities in the 80-120 km height region. The reader is referred to Svoboda et al. (2005) for further information and details.

Figure 12 compares the latitude versus time evolution of DE3 temperature amplitude at 86 km from the work of Svoboda et al. (2005), and that from the present MLS analysis. The similarity between DE3 amplitudes in Figure 12 is striking, and represents a cross-validation of the results and methodologies presented here and in Forbes et al. (2003), and indeed of the HME methodology and our understanding of tidal propagation and dissipation in general. Perhaps the more important implication, however, concerns the controversy between space-based (SB) and ground based (GB, mostly radar) measurements of winds near 95 km altitude (i.e., Burrage, et al., 1996; Meek et al., 1997; Portnyagin et al., 1999; Forbes et al., 2004) that emerged in connection with the UARS mission. Although there is not complete uniformity among these results, in general the

zonal wind measurements from space tend to exceed those from the ground by ~60% near 95 km, with significantly better agreement between measurements for the meridional direction, and for both zonal and meridional winds below 90 km. These results pertain to both instantaneous "overflight" and climatological comparisons between the two data sets. Possible reasons for these differences are discussed in the aforementioned papers, but the issue remains unresolved. The altitude of 95 km is critical, since it is here that both day and night SB data are available, and the zonal wavenumbers of the diurnal tidal components can be unambiguously determined (in an average sense over the 24-hour satellite precession period) with minimal aliasing effects. Establishing consistency between SB and GB measurements is essential if one seeks to take advantage of the space-time sampling attributes of both techniques, and to assimilate these data sets to best establish the dynamical state of the atmosphere at 95 km.

The comparison in Figure 12 provides insight into the above issue. Recall that the temperatures depicted in the lower panel of Figure 12 are based solely on a fit of the first symmetric and first antisymmetric HMEs to DE3 diurnal *wind* structures at 95 km. The fact that the HME temperatures agree well with (and in fact slightly underestimate) the MLS temperature amplitudes (upper panel of Figure 12) is consistent with *no bias* in the HRDI winds, and suggests the source of the SB-GB inconsistency to reside in the GB wind measurements. Of course, this assumes that the MLS temperatures are unbiased, and the HMEs to embody the correct temperature-wind relationship between 86 and 95 km, which depends to some degree on the assumed background temperature, density and dissipation assumed in the HME calculations. Thus the above claim cannot be asserted definitively, but the result is interesting and useful nonetheless.

7. Conclusions

- Analyses of temperatures measured between 25 and 86 km by the Microwave Limb Sounder (MLS) experiment on the Upper Atmosphere Research Satellite (UARS) reveal the presence of migrating (sun-synchronous) and nonmigrating solar tides. Emphasis is placed on the MLS upper altitude limit of 86 km where amplitudes are largest and aliasing effects are minimized. Our results are as follows:

- DW1 amplitudes maximize near the equinoxes and between ±40° latitude with amplitudes of order 10 K. Significant amplitudes (2-4 K) also exist at latitudes of order 60-70°, indicating the presence of trapped modes, possibly indicative of an in-situ source of excitation (i.e., chemical heating).

- SW2 amplitudes are generally of order 2-4 K during most months over a wide range of latitudes, maximizing at 4 – 6 K at low latitudes during February and during the spring at ±60 latitude.

- Diurnal nonmigrating tides D0 and DW2 exist with maxima near the equator and –50° to –60° latitude of order 3 K. The former feature is indicative of propagating modes, while the latter is associated with trapped components for DW2 and mainly trapped components for D0. The same nonmigrating tidal components with similar latitudinal asymmetry were found in UARS wind measurements at 95 km between ±40° latitude by Forbes et al. (2003). Origins for these waves probably lie in zonally

asymmetric heat sources of unknown origin, or in nonlinear interactions between DW1 and SPW1.

- Semidurnal tides SW1 and SW3 and terdiurnal tides TW2 and TW4 are also revealed, with amplitudes of order 1-2 K. Although relatively low in amplitude at 86 km, these waves are expected to grow to 10-12 K by the time they reach their maxima in the lower thermosphere (~110-140 km) and thus can contribute significantly to the dynamics of this atmospheric regime (for instance, see Angelats i Coll and Forbes, 2002). These tidal components probably arise through nonlinear interactions between the migrating tides SW2 and TW3, and the stationary planetary wave with s = 1 (SPW1).

- DE3 achieves amplitudes of order 3 K at low latitudes during March and July-September. This wave is probably generated by latent heat release due to deep tropical convection. Within the confines of dissipative tidal theory, internal consistency is established between the MLS DE3 temperatures at 86 km and previously derived DE3 winds at 95 km. This result is consistent with no bias in the UARS/HRDI winds at 95 km, suggesting the source of the well-known inconsistency between winds measured from the ground and space to primarily reside in the radar wind measurements.

Appendix: Aliasing due to an Evolving Stationary Planetary Wave

A concern that naturally arises in space-based sampling of atmospheric structures, particularly those that are non-stationary, is that of aliasing; that is, when the energy of

one sampled component leaks into another. Consider an s = 1 stationary planetary wave (SPW) whose amplitude varies with time, i.e., $A(t)\cos\lambda$ (without loss of generality the longitude of maximum is assumed at $\lambda = 0$). In the satellite frame, for sampling over a complete yaw period, any temporal variability maps into local time covering 24 hours:

$$A(t)\big|_{yaw}\cos\lambda \rightarrow A(t_{LT})\big|_0^{24}\cos\lambda \tag{A1}$$

which can then be Fourier-decomposed into sub-harmonics of a solar day:

$$A(t_{LT})\big|_0^{24}\cos\lambda = \sum_{n=1}^{N}\cos n\Omega t_{LT}\cos\lambda = \sum_{n=1}^{N}\cos(n\Omega t_{LT} \pm \lambda) \tag{A2}$$

where $\Omega = 2\pi\text{day}^{-1}$ and time is in days. Transforming to canonical form for atmospheric oscillations by letting $t_{LT} = t + \lambda/2\pi$, we have

$$A(t)\big|_{yaw}\cos\lambda \;\rightarrow\; \sum_{n=1}^{N}\cos[n\Omega t + (n \pm 1)\lambda] \tag{A3}$$

Therefore, a time variation in SPW s = 1, from the satellite perspective, aliases into diurnal tides (n = 1) with zonal wavenumbers s = (n ± 1) = 0, 2; semidiurnal tides (n = 2) with s = 1, 3; terdiurnal tides (n = 3) with s = 2, 4; and so on. The reverse process also holds. That is, time variations in the above non-migrating tides can alias into SPW s = 1. However, the non-migrating tidal amplitudes are considerably smaller in magnitude,

hence the scenario (A1) – (A3) is of the greatest concern.

To gain insight into the potential magnitude of the aliasing effect, the following experiment was performed. The MSISE90 model (Hedin, 1991), with local time variations suppressed, was identically sampled both spatially and temporally as the MLS temperature measurements. The resulting data were analyzed for non-migrating tides in a fashion identical to that described previously for the MLS temperature data. The results for +60°N are shown in Figure A1. The SPW amplitudes are of order 2-10 K with maximum values during local winter and spring. The other panels illustrate the derived diurnal s = 0, semidiurnal s = 1 and terdiurnal s = 2 amplitudes that arise from data sampling, which are also representative of results for the diurnal s = 2, semidiurnal s = 3 and terdiurnal s = 4 components. The non-migrating tidal amplitudes are of order 0.2-0.4 K for diurnal and terdiurnal, and 0.2-1.0 K for semidiurnal s = 1. Maxima tend to occur during periods of greatest variation in s = 1 SPW amplitudes over a yaw cycle, i.e., November, January, and April – June. As a general rule, the amplitudes of nonmigrating tides due to aliasing by an evolving SPW do not exceed 10% of the SPW amplitudes. Assuming evolution of the s = 1 SPW in MSISE90 is realistic, this result can be used as a guide for assessing potential aliasing contributions in the actual MLS temperature data set. Note that because we are compositing multiple years of data into a single effective yaw cycle prior to analysis, year-to-year variability may be diminishing the coherence of the seasonal evolution of the s = 1 SPW over the fitting interval. In addition, because MLS views 90 deg from the orbital plane, the local times at the tangent point differ by ~3 h before and after a yaw. This "irregular" sampling helps to reduce the aliasing. The

contributions of both of these effects reducing the potential for aliasing that would exist during a single season.

Acknowledgments. The authors thank Ms. Xiaoli Zhang for her assistance in data processing and figure preparation. This work was supported under Grant FA9550-05-1-0071 from the Air Force Office of Scientific Research to the University of Colorado.

References

Angelats i Coll, M., and J.M. Forbes, 2002: Nonlinear interactions in the upper atmosphere: The s = 1 and s = 3 nonmigrating semidiurnal tides, *J. Geophys. Res*., **107,** 1157, doi:10.1029/2001JA900179.

Burrage, M.D., et al., 1996: Validation of mesosphere and lower thermosphere winds from the High Resolution Doppler Imager on UARS, *J. Geophys. Res*., **101**, 10,365-10,392.

Chapman, S., and R.S. Lindzen, 1970: Atmospheric Tides: Thermal and Gravitational, Gordon and Breach, New York, 200 pp.

Conrath, B.J., 1976: Influence of planetary-scale topography on the diurnal thermal tide during the 1971 Martian dust storm, *J. Atmos. Sci*., **33**, 2430-2439.

Ekanayake, E.M.P., Aso, T., and S. Miyahara, 1997: Background wind effect on propagation of nonmigrating diurnal tides in the middle atmosphere, *J. Atmos. Solar-Terr. Phys*., **59,** 401-429.

Forbes, J.M., 1982: Atmospheric tides 2. The Solar and lunar semidiurnal components, *J. Geophys. Res*., **87**, 5241-5252.

Forbes, J.M., Hagan, M.E., 1982: Thermospheric extensions of the classical expansion functions for semidiurnal tides. *J. Geophys. Res*. **87**, 5253-5259.

Forbes, J.M., M.E. Hagan, X. Zhang and K. Hamilton, 1997: Upper atmosphere tidal oscillations due to latent heat release in the tropical troposphere, *Ann. Geophys*., **15**, 1165-1175.

Forbes, J.M., Kilpatrick, M., Fritts, D., Manson, A., and R. Vincent, 1997: Zonal mean and tidal dynamics from space: an examination of aliasing and sampling issues, *Ann. Geophys.*, **15**, 1158-1164.

Forbes, J. M., N. A. Makarov, and Yu. I. Portnyagin, 1995: First results from the meteor radar at South Pole: A large 12-hour oscillation with zonal wavenumber one, *Geophys. Res. Lett.*, **22**, 3247-3250.

Forbes, J.M., Yu.I. Portnyagin, N.A. Makarov, S.E. Palo, E.G. Merzlyakov, and X. Zhang, 1999: Dynamics of the lower thermosphere over South Pole from meteor radar wind measurements, *Earth, Planets and Space,* **51**, 611-620.

Forbes, J.M. and F. Vial, 1989: Monthly Simulations of the Solar Semidiurnal Tide in the Mesosphere and Lower Thermosphere, *J. Atmos. Terr. Phys*., **51**, 649-662.

Forbes, J.M., and F. Vial, 1991: Semidiurnal tidal climatology of the E Region, *J. Geophys. Res.*, **96**, 1147-1157.

Forbes, J.M., Manson, A.H., Vincent, R.A., Fraser, G.J., Vial, F., Wand, R., Avery, S.K., Clark, R.R., Johnson, R., Roper, R., Schminder, R., Tsuda, T., and E.S. Kazimirovsky, 1994: Semidiurnal Tide in the 80-150 km Region: An Assimilative Data Analysis, *J. Atmos. Terr. Phys*., **56**, 1237-1250.

Forbes, J.M., X. Zhang, and M.E. Hagan, 2001: Simulations of diurnal tides due to tropospheric heating from the NCEP/NCAR Reanalysis Project, *Geophys. Res. Lett*., **28**, 3851-3854.

Forbes, J.M., Zhang, X., Ward, W., and E. Talaat, 2003: Nonmigrating diurnal tides in the thermosphere, *J. Geophys. Res*., **108**, 1033, doi:10.1029/2002JA009262.

Forbes, J. , Portnyagin, Yu. , Skinner, W. , Vincent, R. , Solovjova, T. , Merzlyakov, E. , Nakamura, T. , and Palo, S., 2004: Climatological lower thermosphere winds as seen by ground-based and space-based instruments, *Ann. Geophys*., 1432-0576/ag/2004-22, 1931.

Grieger, N. et al., 2002: General circulation model results on migrating and nonmigrating tides in the mesosphere and lower thermosphere. Part I: Comparison with observations, *J. Atmos. Solar-Terr. Phys*, 897–911.

Grieger, N., G. Schmitz, and U. Achatz, 2004: The dependence of nonmigrating diurnal tide in the mesosphere and lower thermosphere on stationary planetary waves, *J. Atmos. Solar-Terr. Phys.*, **66**, 733-754.

Hagan, M. E., J. L. Chang, and S. K. Avery, 1997: GSWM estimates of nonmigrating tidal effects, *J. Geophys. Res*., **102**, 16,439– 16,452.

Hagan, M.E., McLandress, C., and J.M. Forbes, 1997: Diurnal tidal variability in the upper mesosphere and lower thermosphere, *Ann. Geophys*., **15**, 1176-1186.

Hagan, M.E., and R.G. Roble, 2001: Modeling diurnal tidal variability with the NCAR TIME-GCM, *J. Geophys. Res*., **106**, 24869-24882.

Hagan, M.E., and J.M. Forbes, 2002: Migrating and nonmigrating diurnal tides in the middle and upper atmosphere excited by tropospheric latent heat release, *J. Geophys. Res.*, **107**, 4754, doi:10.1029/2001JD001236.

Hagan, M.E., and J.M. Forbes, 2003: Migrating and nonmigrating semidiurnal tides in the middle and upper atmosphere excited by tropospheric latent heat release, *J. Geophys. Res*., **108**, 1062, doi:10.1029/2002JA009466.

Hedin, A.E., 1991: Extension of the MSIS thermosphere model into the middle and lower atmosphere, *J. Geophys. Res*., **96**, 1159-1172.

Hendon, H. H., and K. Woodberry, 1993: The diurnal cycle of tropical convection, *J. Geophys. Res*., **98**, 16,623-16,637.

Lieberman, R.S., J. Oberheide, M.E. Hagan, E.E. Remsberg, and L.L. Gordley, 2004: Variability of diurnal tides and planetary waves during November 1978 – May 1979, *J. Atmos. Solar-Terr. Phys*., **66**, 517-528, doi: 10.1016/j.jastp.2004.01.006.

Lieberman, R. S., 1991: Nonmigrating diurnal tides in the equatorial middle atmosphere, *J. Atmos. Sci*., **48**, 1112–1123.

Lindzen, R.S., and S.-S. Hong, 1974: Effects of mean winds and horizontal temperature gradients on solar and lunar semidiurnal tides in the atmosphere, *J. Atmos. Sci*., **31**, 1421-1446.

Lindzen, R.S., 1976: A modal decomposition of the semidiurnal tide in the lower thermosphere, *J. Geophys. Res*., **81**, 2923-2926.

Lindzen, R.S., S.-S. Hong, and J.M. Forbes, 1977: Semidiurnal Hough mode extensions into the thermosphere and their application, *Memo. Rept.* **3442**, Naval Res. Lab., Wash., D.C.

Manson, A.H., Luo, Y., and Meek, C., 2002: Global Distributions of Diurnal and semi-Diurnal Tides: Observations from HRDI-UARS of the MLT Region, *Annales Geophysicae*, **20**, 1877-1890.

Meek, C.E., Manson, A.H., Burrage, M.D., Garbe G., and Cogger, L.L., 1997: Comparisons between Canadian Prairie MF Radars, FPI (green and OH Lines) and UARS HRDI systems, *Annales Geophysicae*, **15**, 1099-1110.

Miyahara, S. and Y. Miyoshi, 1997: Migrating and nonmigrating atmospheric tides simulated by a middle atmosphere general circulation model, *Adv. Space Res*., **20**, 1201–1207.

Miyahara, S., Y. Miyoshi, and K. Yamashita, 1999: Variations of migrating and nonmigrating tides simulated by the middle atmosphere circulation model at Kyushu University, *Adv. Space Res*., **24**, 1549–1558.

Mlynczak, M.G., and S. Solomon, 1993: A detailed evaluation of the heating efficiency in the middle atmosphere, *J. Geophys. Res*., **98**, 10517-10541.

Oberheide, J., M. E. Hagan, R. G. Roble, and D. Offermann, 2002: Sources of nonmigrating tides in the tropical middle atmosphere, *J. Geophys. Res*., **107**, 4567, doi:10.1029/2002JD002220.

Oberheide, J., and O.A. Gusev, 2002: Observation of migrating and nonmigrating diurnal tides in the equatorial lower thermosphere, *Geophys. Res. Lett*., **29**, 2167, doi:10.1029/2002GL016213.

Portnyagin, Yu.I., Solovjova, T.V., and Wang, D.Y., 1999: Some results of comparison between the lower thermosphere zonal winds as seen by the ground-based radars and WINDII on UARS, *Earth, Planets and Space*, **51**, 701-709.

Portnyagin, Yu. I., J. M. Forbes, N. A. Makarov, E. G. Merzlyakov, S. Palo, 1998: The summertime 12-hour wind oscillation with zonal wavenumber s = 1 in the lower thermosphere over South Pole, *Ann. Geophys*., **16**, 828-837.

Smith, A.K., Structure of the terdiurnal tide at 95 km, 2000: *Geophys. Res. Lett.*, **27**, 177-200.

Smith, A.K., and Ortland, D.A., 2001: Modeling and analysis of the structure and generation of the terdiurnal tide, *J. Atmos. Sci.*, **58**, 3116-3134.

Smith, A.K., D.R. Marsh, and A.C. Szymczak, 2003: Interaction of chemical heating and the diurnal tide in the mesosphere, *J. Geophys. Res.*, **108**, 4164, doi:10.1029/2002JD002664.

Svoboda, A.A., Forbes, J.M., and S. Miyahara, 2005: A Space-Based Climatology of MLT Winds, Temperatures and Densities from UARS Wind Measurements, J. Atmos. Solar-Terr. Phys, submitted.

Talaat, E.R., and R. S. Lieberman, 1999: Nonmigrating diurnal tides in mesospheric and lower thermospheric winds and temperatures, *J. Atmos. Sci.*, **56**, 4073-4087.

Teitelbaum, H. and F. Vial, 1991: On tidal variability by nonlinear interaction with planetary waves, *J. Geophys. Res*. **96**, 14,169–14,178.

Tokioka, T. and I. Yagai, 1987: Atmospheric tides appearing in a global atmospheric general circulation model, *J. Meteor. Soc. Japan*, **65**, 423–437.

Williams, C. R., and S. K. Avery, 1996: Diurnal nonmigrating tidal oscillations forced by deep convective clouds, *J. Geophys. Res*., **101**, 4079-4091.

Wu, D.L., et al., 2003: Mesospheric temperature from UARS MLS: retrieval and validation, *J. Atmos. Solar-Terr. Phys*., **65**, 245-267.

Yagai, I., 1989: Nonmigrating thermal tides detected in data analysis and a general circulation model simulation, *J. Geophys. Res*., **94**, 6341-6356.

Yamashita, K., Miyahara, S., Miyoshi, Y., Kawano, K., and J. Ninomiya, 2002: Seasonal variation of non-migrating semidiurnal tide in the polar MLT region in a general circulation model, *J. Atmos. Sol.-Terr. Phys*., 1083-1094.

Zurek, R.W., 1976: Diurnal tide in the Martian atmosphere, *J. Atmos. Sci*., **33**, 321-337.

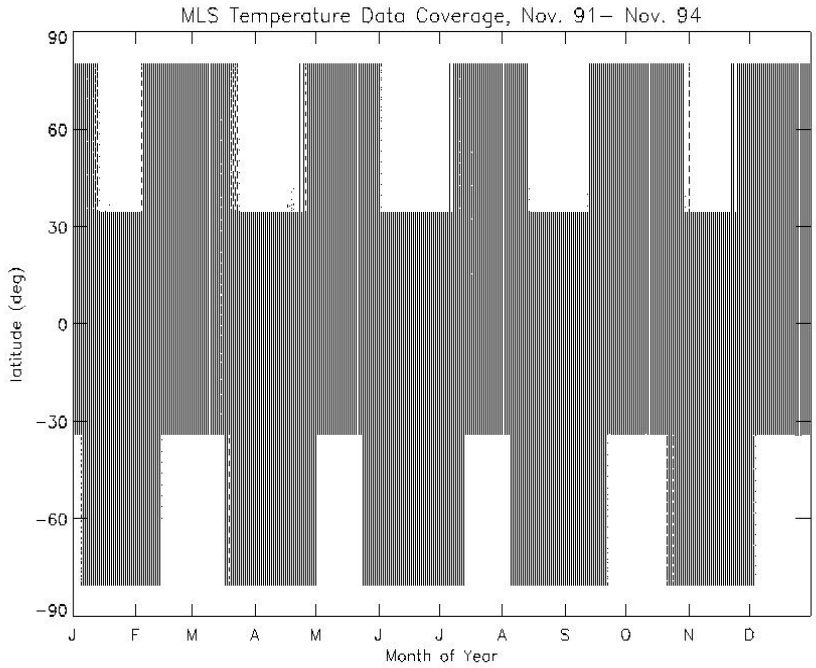

Figure 1. MLS data coverage for the period November, 1991 – November, 1994.

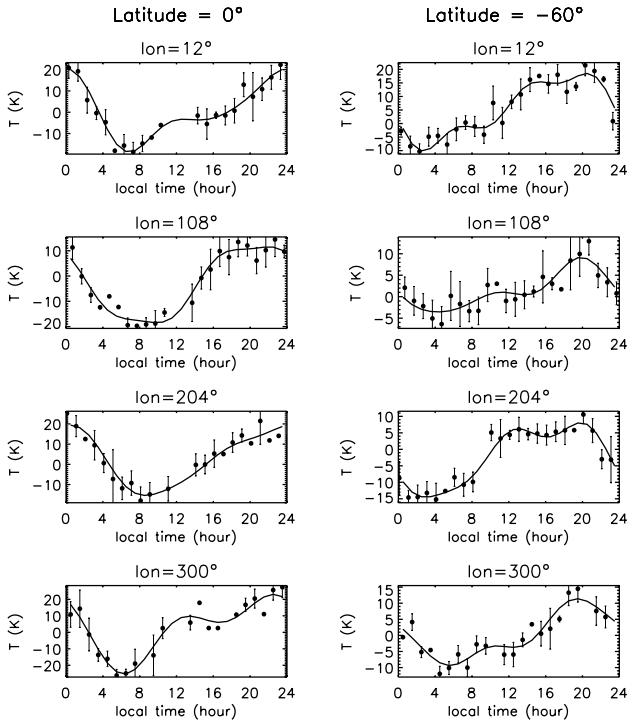

Figure 2. Temperature differences from zonal mean, March at 86 km, for longitudes 12°, 108°, 204°, and 300° (top to bottom), for latitudes 0° (left) and -60° (right).

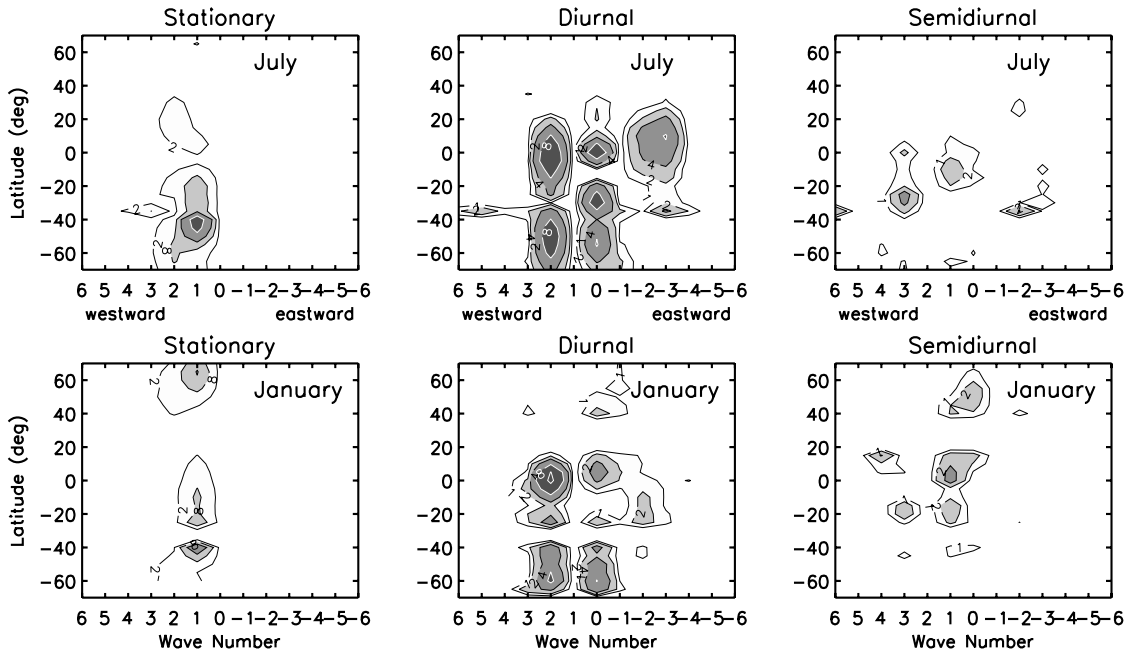

Figure 3. Power spectra for temperature at 86 km for stationary (left), diurnal (middle) and semidiurnal (right) components as a function of latitude and zonal wavenumber (positive westward) for July (top) and January (bottom).

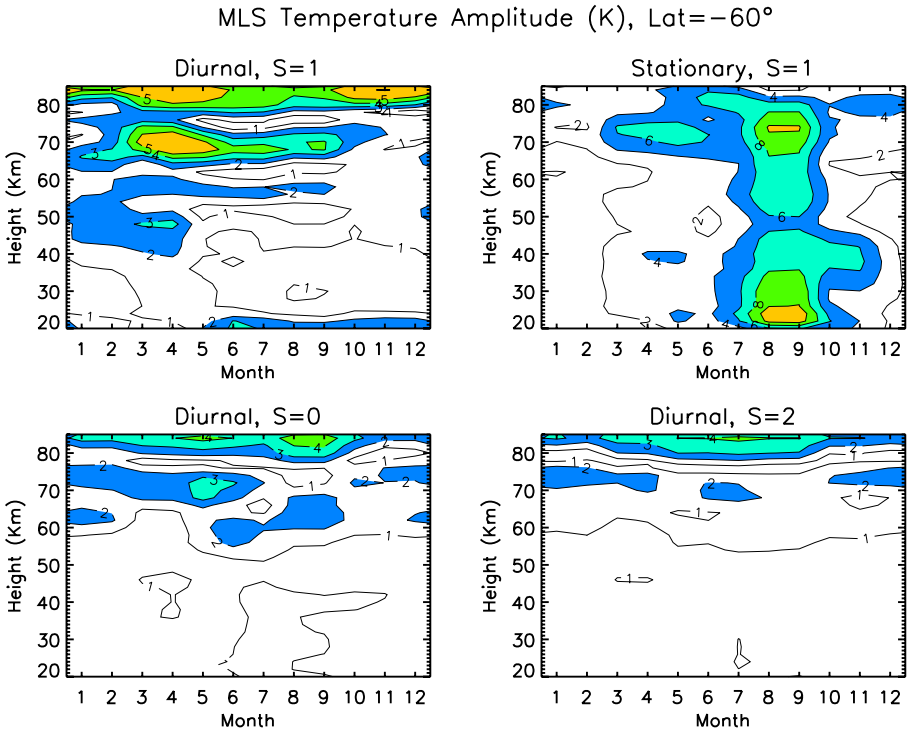

Figure 4. Height vs. month structures of temperature amplitude for DW1 (top left), SPW1 (top right), D0 (bottom left), and DW2 (bottom right) as a function of height and month at -60° latitude.

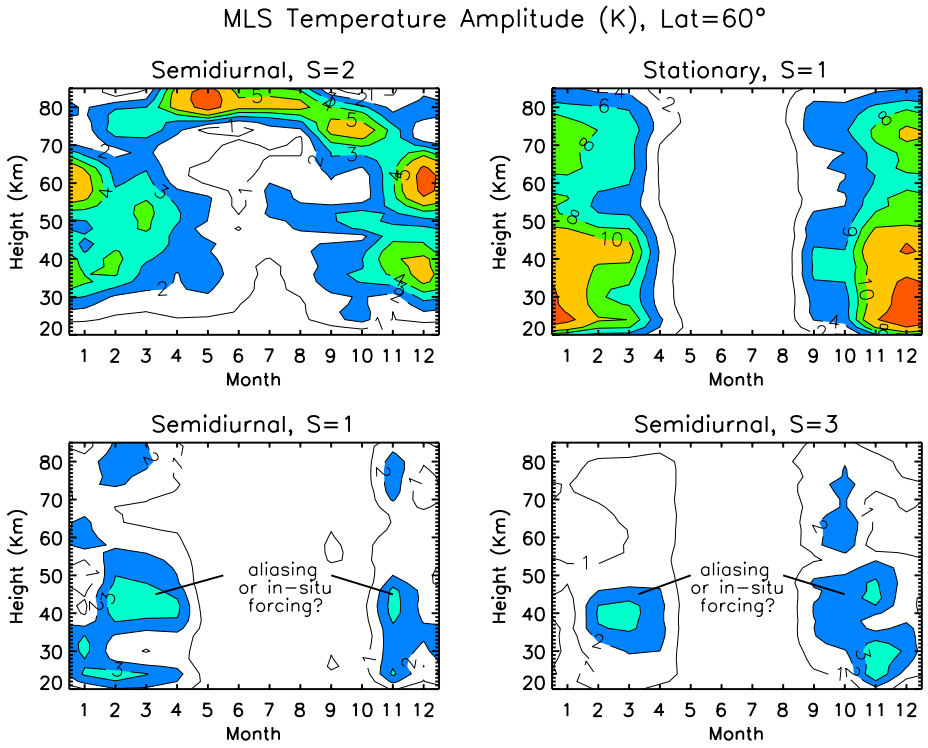

Figure 5. Height vs. month structures of temperature amplitude for SDW2 (top left), SPW1 (top right), SDW1 (bottom left), and SDW3 (bottom right) as a function of height and month at +60° latitude.

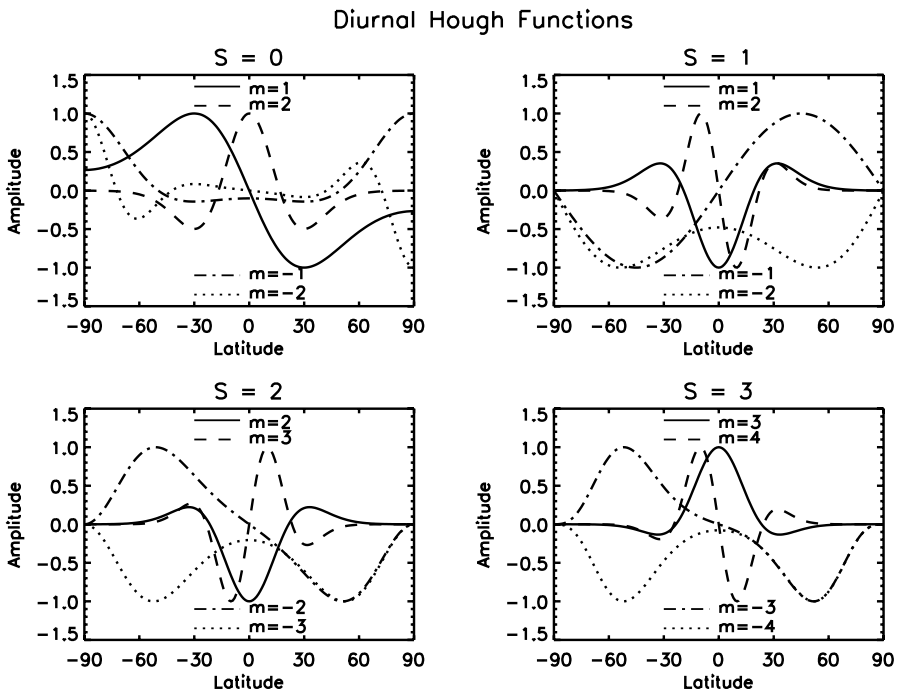

Figure 6. Diurnal Hough functions for zonal wavenumbers s = 0, 1, 2, 3.

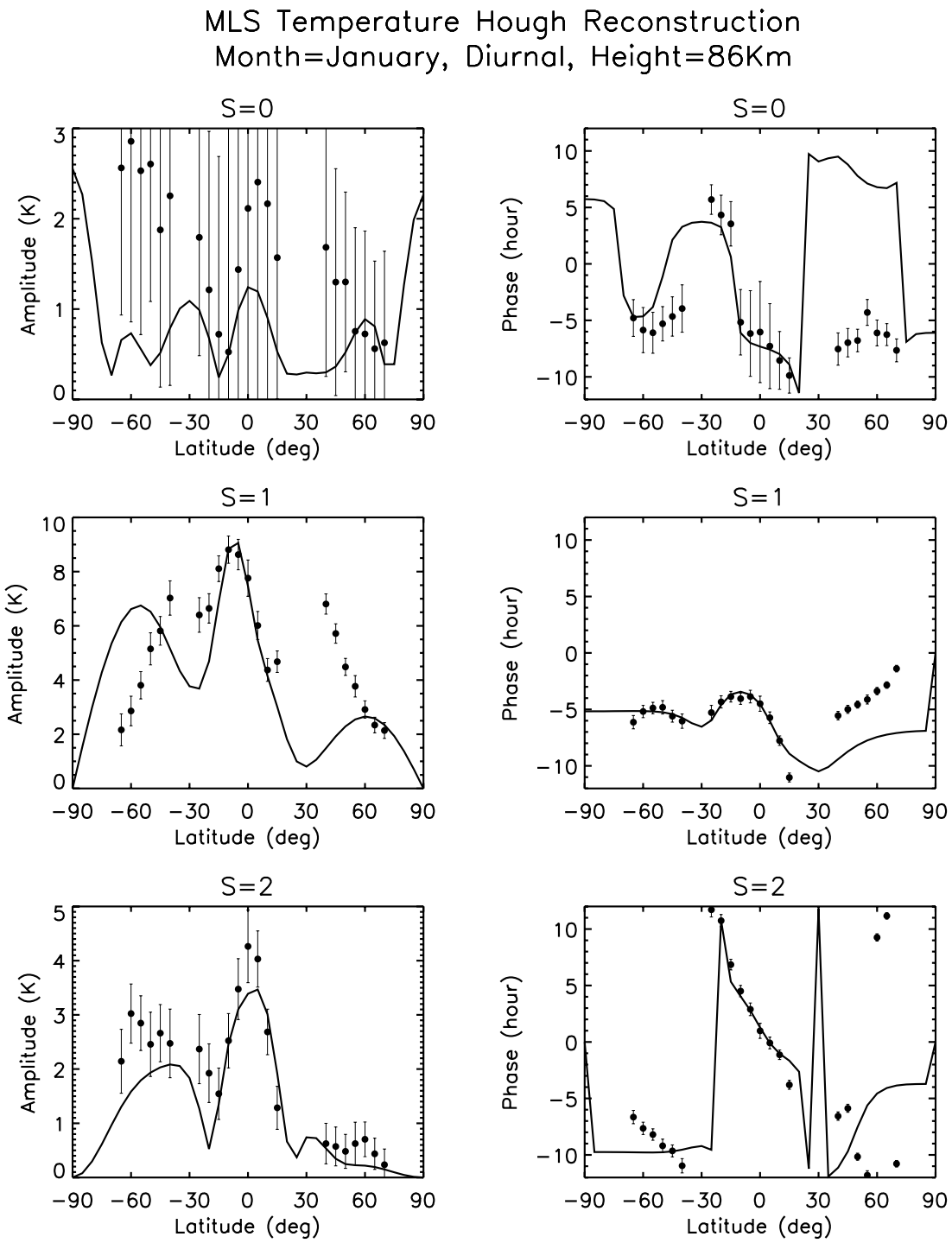

Figure 7. Latitude structures of January temperature amplitude (left) and phase (right) at 86 km altitude for D0 (top), DW1 (middle) and DW2 (bottom). The solid lines represent Hough mode fits to these data taking into account the first symmetric and anti-symmetric propagating and trapped modes.

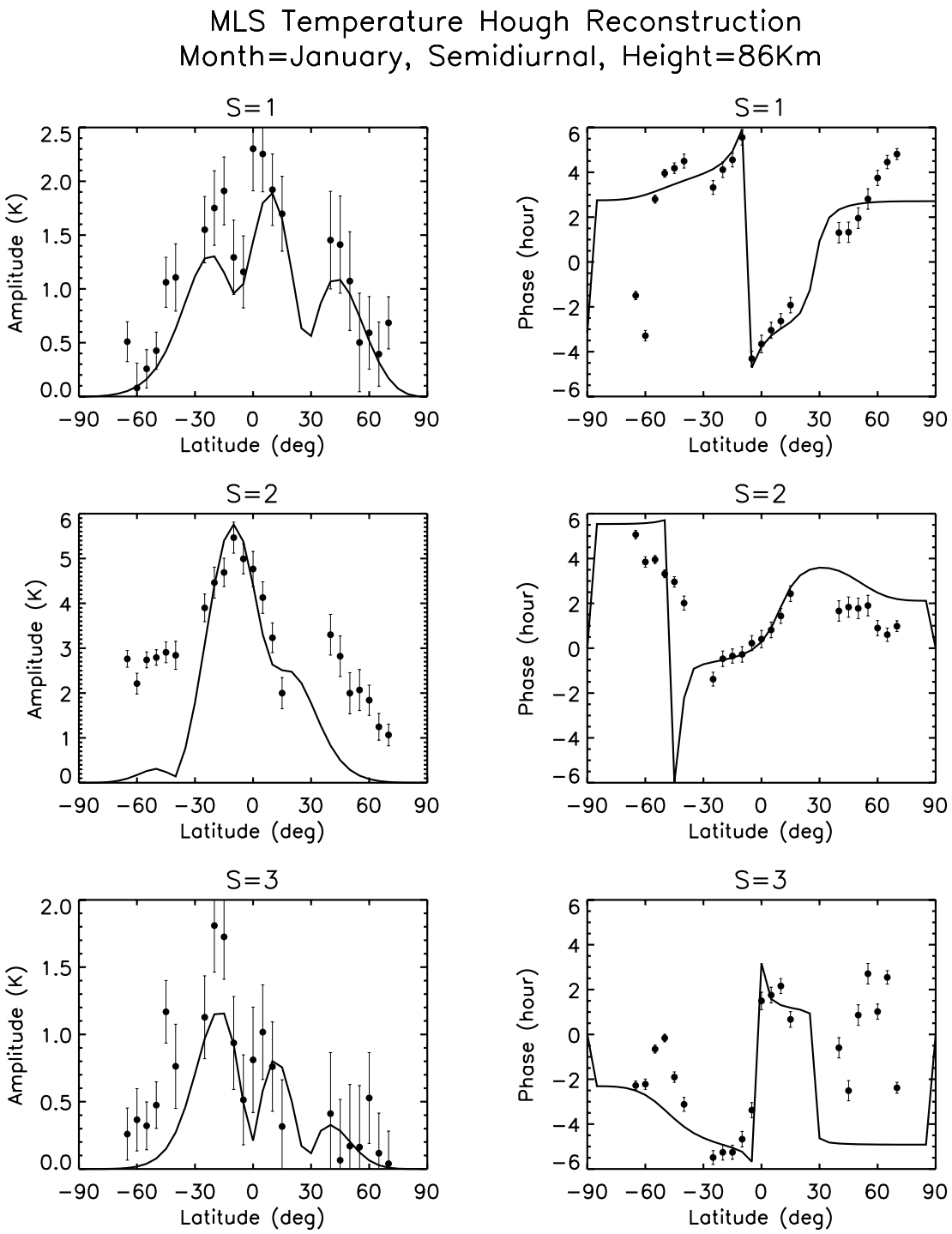

Figure 8. Same as Figure 7, except for SDW1, SDW2 and SDW3.

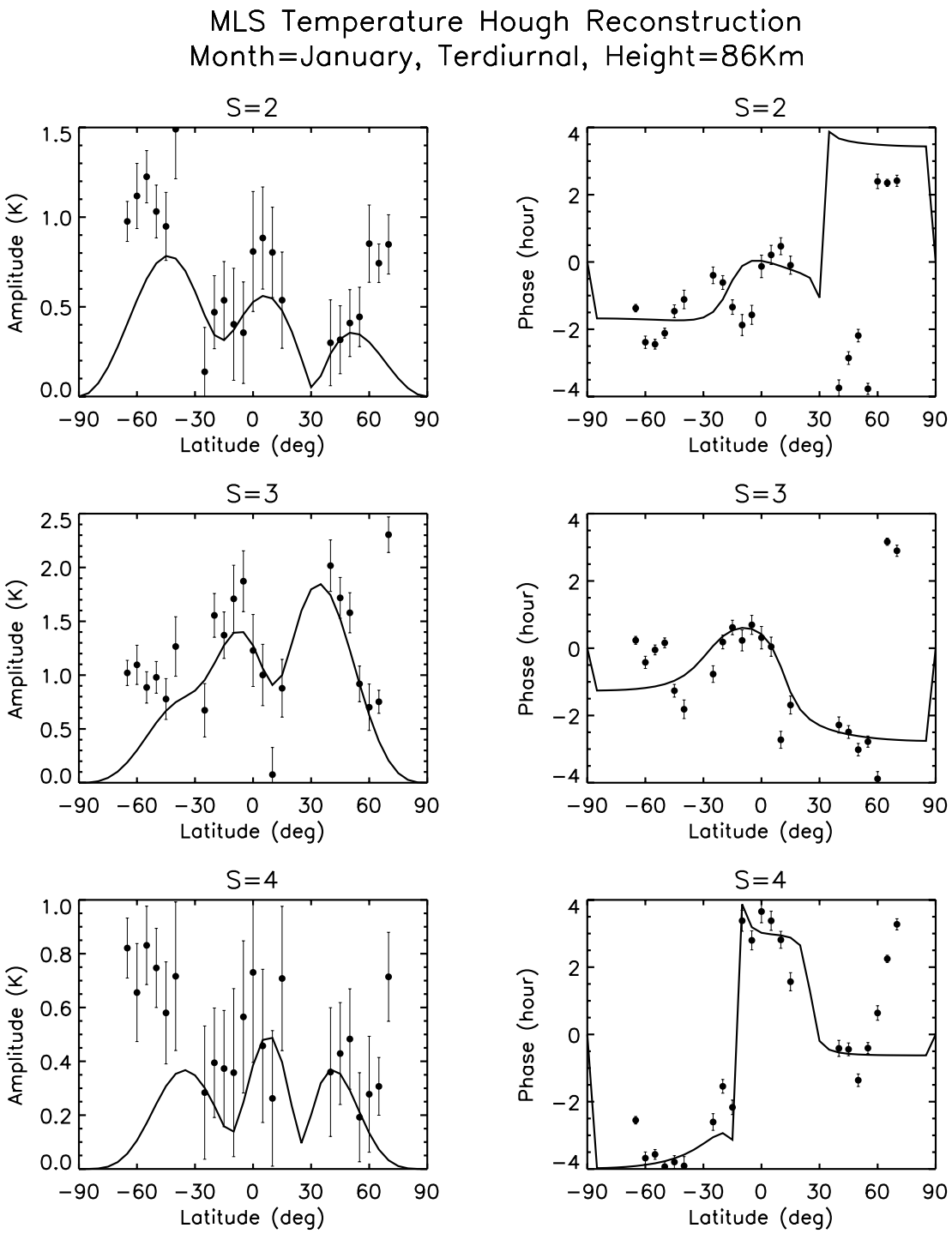

Figure 9. Same as Figure 7, except for TDW2, TDW3 and TDW4.

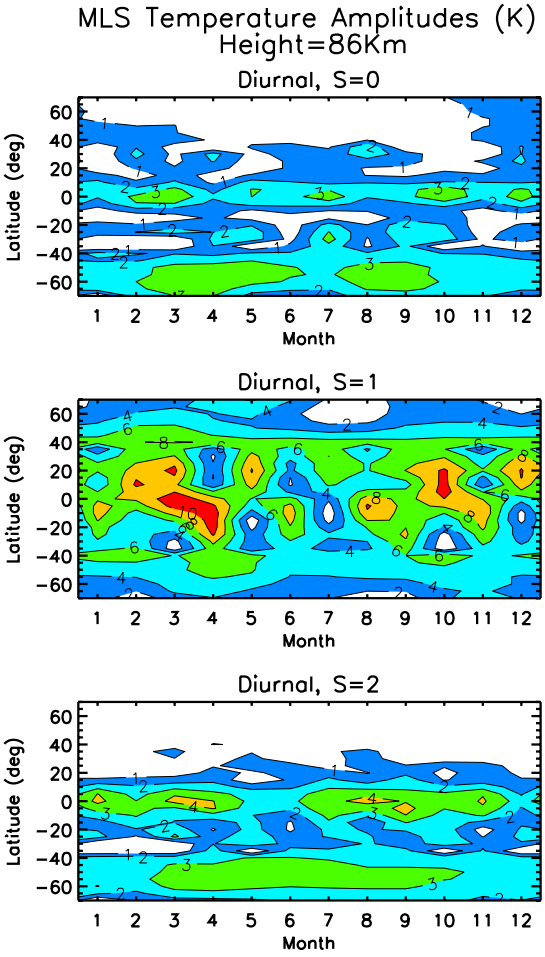

Figure 10. Latitude versus month contours of D0, DW1 and DW2 diurnal temperature amplitudes at 86 km.

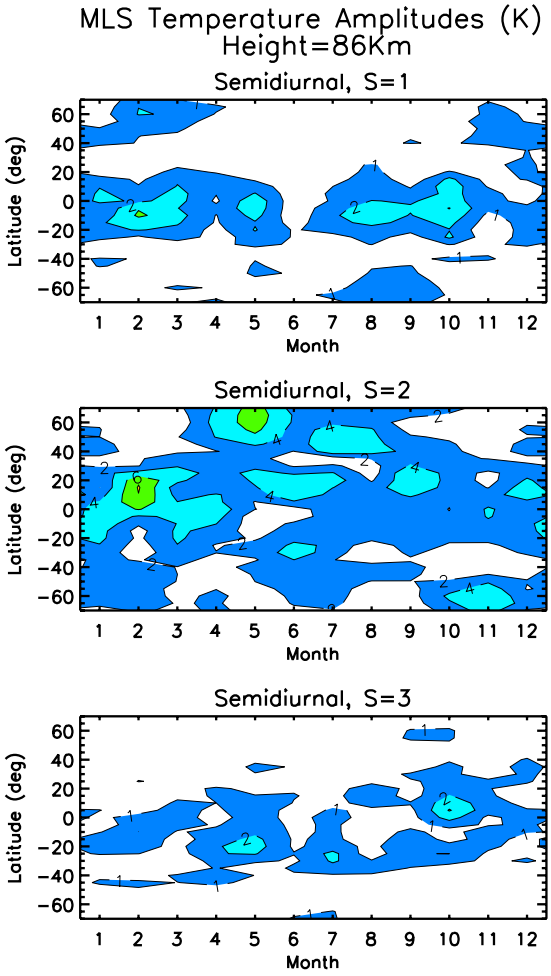

Figure 11. Same as Figure 10, except for SDW1, SDW2, and SDW3.

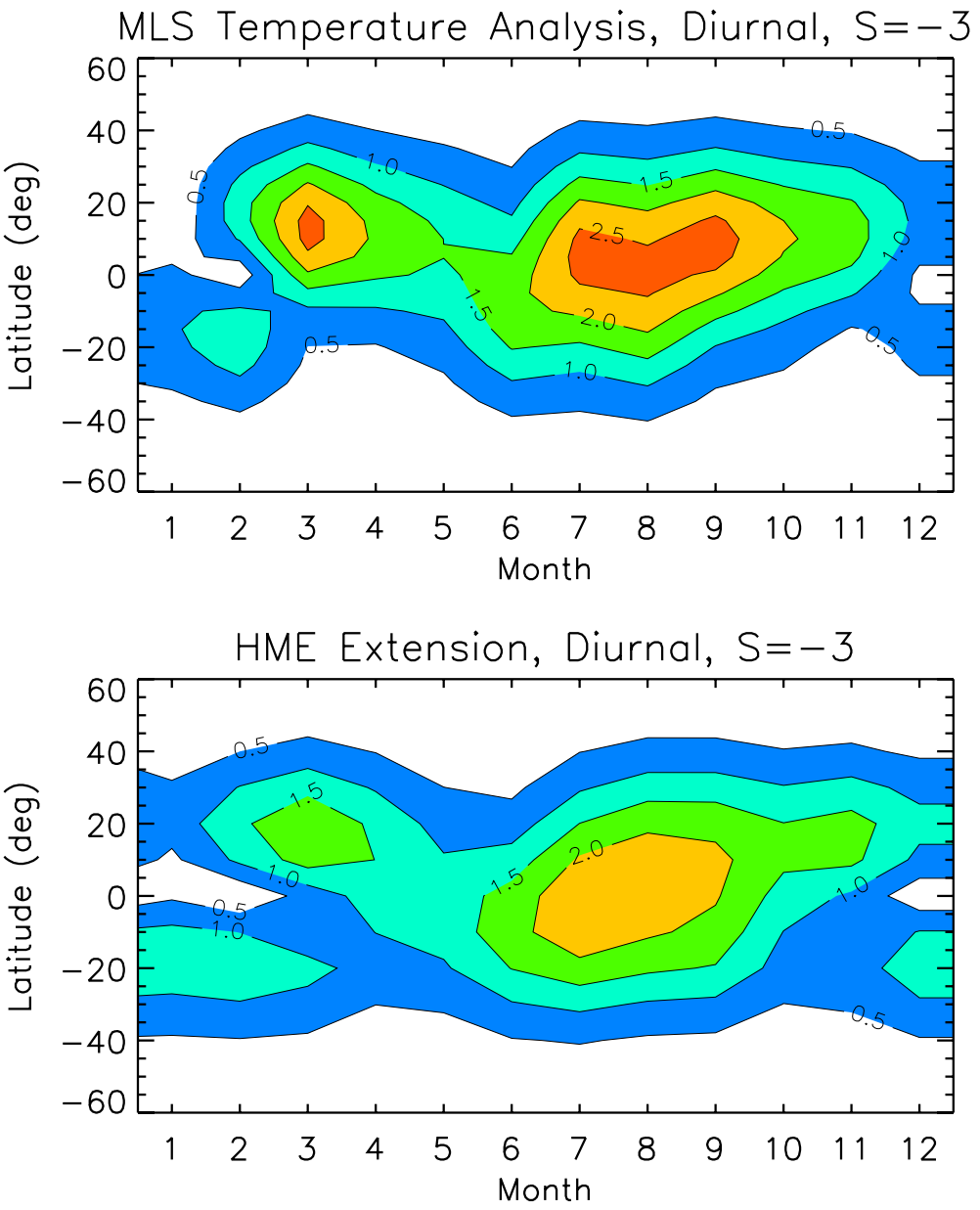

Figure 12. Latitude versus month contours of DE3 diurnal temperature amplitudes. Top: From present analysis of MLS temperatures. Bottom: Derived from HME fit to DE3 eastward and northward winds at 95 km from UARS WINDII and HRDI measurements (Forbes et al., 2003).

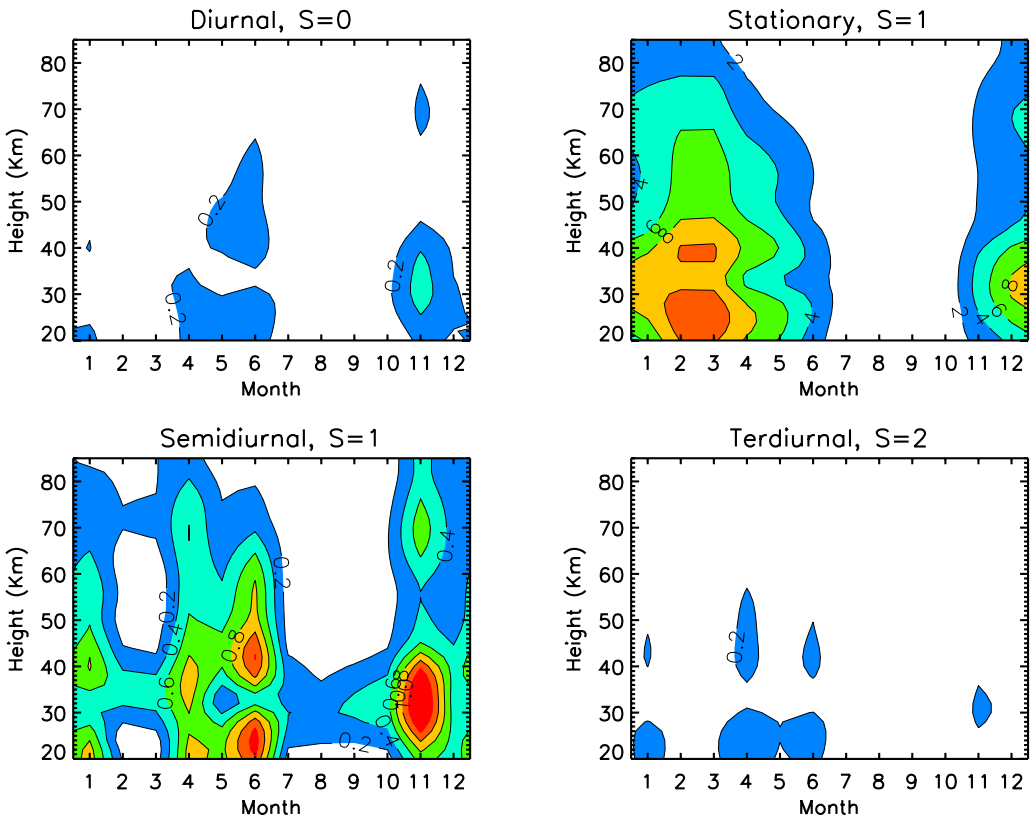

Figure A1. Amplitudes of DW2 (top left), SPW1 (top right), SDW1 (bottom left) and TDW2 (bottom right) as a function of height and month, obtained by sampling the MSISe90 model (with local time variations suppressed) according to the MLS temperature measurements during November, 1991 – November, 1994. The tidal components primarily reflect aliasing due to SPW1 variability over the 36-day fitting intervals.